

DOI: [10.29026/oes.2023.230018](https://doi.org/10.29026/oes.2023.230018)

Smart Palm-size Optofluidic Hematology Analyzer for automated imaging-based leukocyte concentration detection

Deer Su¹, Xiangyu Li², Weida Gao³, Qihua Wei⁴, Haoyu Li¹, Changliang Guo^{5,6*} and Weisong Zhao^{1*}

¹Innovation Photonics and Imaging Center, School of Instrumentation Science and Engineering, Harbin Institute of Technology, Harbin 150080, China; ²Department of Control Science and Engineering, Harbin Institute of Technology, Harbin 150081, China; ³Department of neurosurgery, The Second Affiliated Hospital of Harbin Medical University, Harbin 150086, China; ⁴Institute of Optical Measurement and Intellectualization, Harbin Institute of Technology, Harbin 150080, China; ⁵Beijing Institute of Collaborative Innovation, Beijing 100094, China; ⁶State Key Laboratory of Membrane Biology, Beijing Key Laboratory of Cardiometabolic Molecular Medicine, Institute of Molecular Medicine, National Biomedical Imaging Center, School of Future Technology, Peking University, Beijing 100871, China.

*Correspondence: CL Guo, E-mail: changguo@gmail.com; WS Zhao, E-mail: weisongzhao@hit.edu.cn

This file includes:

[Section 1: Linear range analysis of the system](#)

[Section 2: Repeatability analysis of the system](#)

[Section 3: Contrast analysis of the system](#)

[Section 4: The experimental process of cell counting by hemocytometer](#)

[Section 5: Supplementary Video 1](#)

Supplementary information for this paper is available at <https://doi.org/10.29026/oes.2023.230018>



Open Access This article is licensed under a Creative Commons Attribution 4.0 International License.

To view a copy of this license, visit <http://creativecommons.org/licenses/by/4.0/>.

© The Author(s) 2023. Published by Institute of Optics and Electronics, Chinese Academy of Sciences.

Section 1: Linear range analysis of the system

To access the measurement range, we obtained a series of samples of white blood cells with concentration gradients through dilution. Subsequently, we performed 10 repetitions of each test using our device and calculated the standard values, average values, and coefficient of variation (CV) for each dataset (Table S1). As illustrated in Fig. S1(a-c), the determined standard value and the average value satisfied the linear regression equation of $y = 1.0191x - 0.3621$, $y = 1.0202x - 0.0870$, and $y = 0.8885x - 0.6211$, respectively. The regression coefficients were $R = 0.987$, $R = 0.989$, and $R = 0.966$, respectively, indicating a high-level consistency when the detection concentration ranges from $1.52 \times 10^2/\mu\text{L}$ to $12.08 \times 10^2/\mu\text{L}$. On the other hand, at $2 \mu\text{L}/\text{min}$, according to Fig. S1(d), the obtained average values significantly deviated from the standard regression equation, demonstrating a failure case of the method. Because of the severe motion blur effects at a flow rate of $2 \mu\text{L}/\text{min}$, some cells failed to be counted as illustrated in Fig. S1(e).

Table S1 | Standard values, average values, and coefficient of variation (CV) of white blood cell concentration for samples.

Sample number	Average values ($10^2/\mu\text{L}$)	Standard values ($10^2/\mu\text{L}$)	CV (%)
1	1.37	1.52	9.83
2	2.78	3.03	9.76
3	4.84	4.53	8.18
4	6.36	6.04	7.77
5	6.96	7.48	6.53
6	9.52	9.06	6.42
7	10.98	10.49	5.13
8	11.82	12.08	4.21

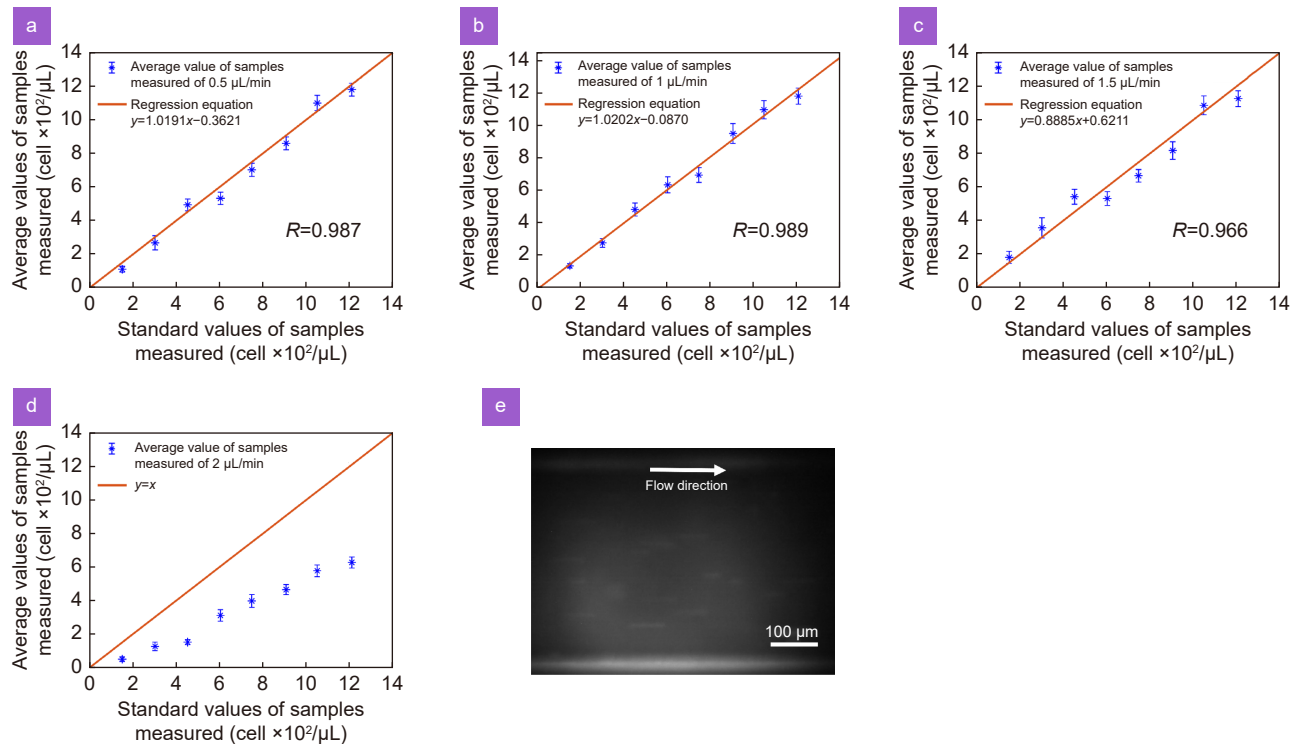


Fig. S1 | The regression equation for the standard value and the average measured value of the samples in Table S1 at different flow rates. (a) At a flow rate of $0.5 \mu\text{L}/\text{min}$, the linear regression equation between $1.52 \times 10^2/\mu\text{L}$ and $12.08 \times 10^2/\mu\text{L}$ is $y = 1.0191x - 0.3621$ with the regression coefficient of $R = 0.987$. **(b)** At a flow rate of $1.0 \mu\text{L}/\text{min}$, the linear regression equation between $1.52 \times 10^2/\mu\text{L}$ and $12.08 \times 10^2/\mu\text{L}$ is $y = 1.0202x - 0.0870$ with the regression coefficient of $R = 0.989$. **(c)** At a flow rate of $1.5 \mu\text{L}/\text{min}$, the linear regression equation between $1.52 \times 10^2/\mu\text{L}$ and $12.08 \times 10^2/\mu\text{L}$ is $y = 0.8885x - 0.6211$ with the regression coefficient of $R = 0.966$. **(d)** The average measured value at a flow rate of $2.0 \mu\text{L}/\text{min}$ and the standard regression equation $y = x$. **(e)** Sample image at a flow rate of $2.0 \mu\text{L}/\text{min}$, partial cells could not be distinguished. Scale bar: $100 \mu\text{m}$.

Section 2: Repeatability analysis of the system

To assess the repeatability, we calculated the CV by taking the standard deviation divided by the mean for ten measurements of each data set. According to Table S1, within the detection range, the CV increases as the sample concentration decreases. At a concentration of $1.52 \times 10^2 / \mu\text{L}$, the CV was at 9.83%, which aligns with results from similar devices^{S1}, demonstrating good reproducibility. In comparison to their cumbersome imaging systems, our device has significant advantages of portability.

Section 3: Contrast analysis of the system

To evaluate the sensitivity of our device from an imaged-based point-of-view, we used the "Root Mean Square Contrast" metric to quantify the sensitivity of our device as illustrated in equation (1). Specifically, the contrast calculation formula was illustrated in the following equation, where I_{ij} is the gray level of one pixel, and \bar{I} is the averaged gray level of an image with $M \times N$ pixels.

$$C = \sqrt{\frac{1}{MN} \sum_{i=0}^{N-1} \sum_{j=0}^{M-1} (I_{ij} - \bar{I})^2}. \quad (1)$$

We analyzed the contrast of particles resolved in the image before our pre-processing process. A representative frame is shown in Fig. S2(a), and the 8 particles at the edge of the field of view and with the weakest signal-to-noise ratio were highlighted and numbered in blue boxes (Fig. S2(b)). The contrast values of particles were calculated, and the Cell #7 was with the lowest contrast of 7.27. This suggests that the particle with a contrast value of at least 7.27 can be identified, reflecting the good sensitivity of our device.

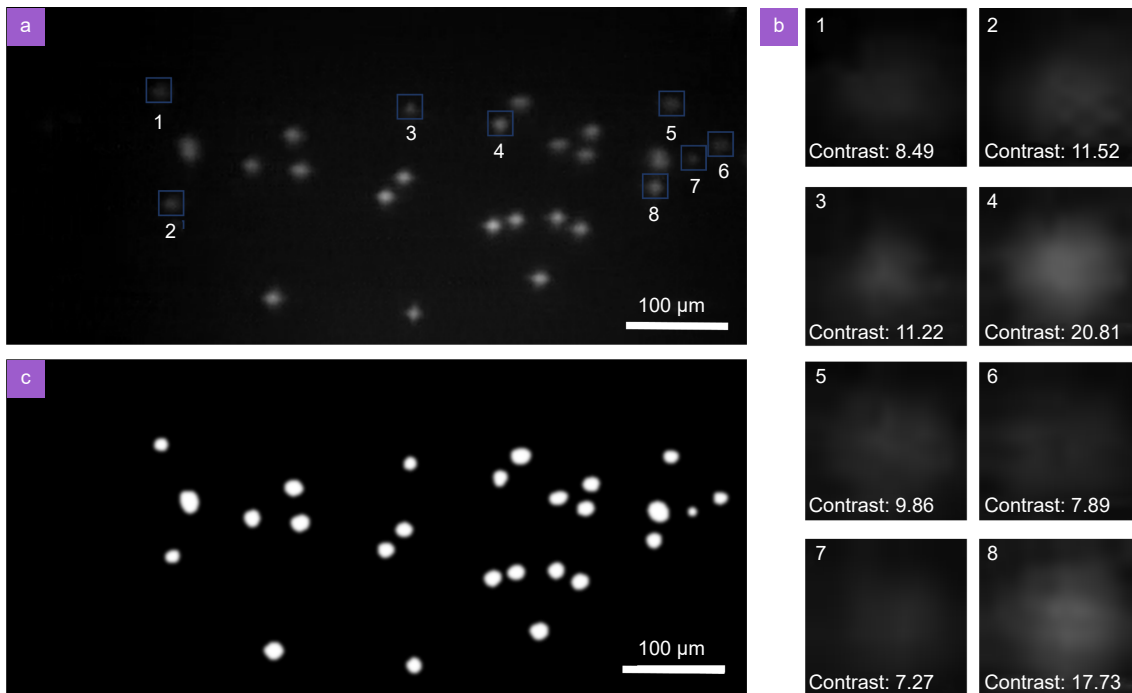


Fig. S2 | (a) The image of cells during flow, where a portion of cells with lower contrast is boxed in blue and labeled with a serial number. (b) Magnified view of the cells in the blue box of (a) and the corresponding contrast. (c) The image obtained after preprocessing. Scale bar: 100 μm .

Section 4: The experimental process of cell counting by hemocytometer

We used a hemocytometer for manual cell counting under a microscope. As shown in Fig. S3, the stained and diluted blood sample was dropped onto the hemocytometer and placed under a microscope. Particle counts were performed on the squares in the middle and corners, and the counted result C was used to calculate the cell concentration M by the following equation, where N represents the dilution ratio. Each sample group was counted ten times, and the average value was obtained.

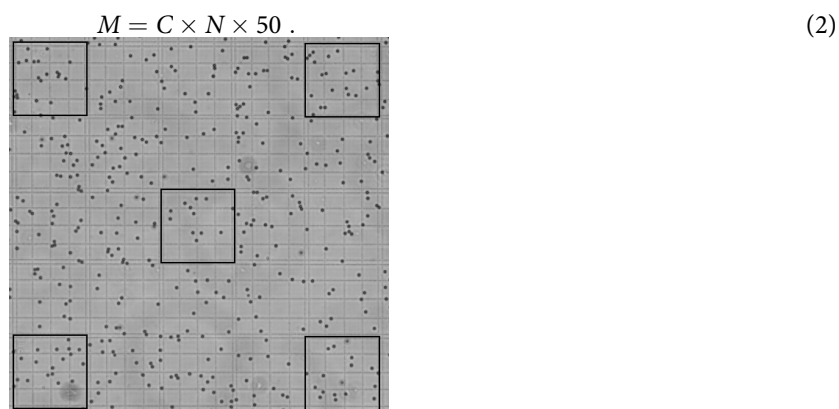


Fig. S3 | Counting result of hemocytometer by a microscope.

Section 5: Supplementary Video 1

The Supplementary Video 1 demonstrates the process of cell counting using our Palm-size Optofluidic Hematology Analyzer at a flow rate of 1 $\mu\text{L}/\text{min}$.

References

- S1. Kim B, Oh S, Shin S, Yim SG, Yang SY et al. Pumpless microflow cytometry enabled by viscosity modulation and immunobead labeling. *Anal Chem* **90**, 8254–8260 (2018).